Synthesis of p-type $Mg_2Si_{1-x}Sn_x$ with x = 0-1 and optimization of the synthesis parameters

H. Kamila[a*], A. Sankhla[a], M. Yasseri[a,b], N. P. Hoang[a], N. Farahi[a], E. Mueller[a,b], J. de Boor[a*]

[a] *Institute of Materials Research, German Aerospace center, Linder Hoehe, Cologne 51147, Germany*

[b] *Institute of Inorganic and Analytical Chemistry, Justus Liebig University Giessen, Giessen 35392, Germany*

Abstract

Mg_2Si is a promising thermoelectric material in the mid-temperature region 500 – 800 K. Development of Mg_2Si based thermoelectric generators requires both good n- and p-type materials. While the thermoelectric properties n-type $Mg_2(Si,Sn)$ materials are good, those of the corresponding p-type are not as much. Therefore, optimizing p-type solid solution of magnesium silicide and magnesium stannide is highly desired. We employ high energy ball milling for efficient synthesis of p-type $Mg_2(Si,Sn)$ and investigate the effect of milling time, sintering temperature, and holding time on the thermoelectric properties of p-type $Mg_2Si_{1-x}Sn_x$ with x = 0-1. We can show the synthesis of p-type $Mg_2(Si,Sn)$ for the whole compositions using Li as a dopant. We have also studied the effect of the synthesis parameters (milling time, sintering temperature, and holding time) on the phase purity, functional homogeneity and thermoelectric properties. The phase purity increases with longer milling time. The functional homogeneity decreases with higher sintering temperature and longer holding time. The optimum synthesis condition for x = 0.6 leads to zT_{max} ~ 0.6 at 700 K, which is one of the highest value reported for p-type $Mg_2(Si,Sn)$.

1. Introduction

Thermoelectric materials can convert waste heat into electricity. Developing thermoelectric generators is promising for several applications such as launcher, cars, and deep space probes [1, 2]. The efficiency of thermoelectric generators depends on the figure of merit of the constituting materials given by $zT = S^2 \sigma/\kappa T$. Here S, σ, and κ are Seebeck coefficient, electrical conductivity, and thermal conductivity, respectively. Mg_2Si and its solid solutions are very attractive due to their good thermoelectric performance in the mid-temperature region 500 – 800 K, environment compatibility, non-toxicity, abundance and low cost of

materials [3-5].

Development of Mg_2Si based thermoelectric generators requires both good p- and n-type materials. For n-type, good thermoelectric properties have been reported for binary Mg_2Si with zT~1 [6, 7], and particularly for solid solutions with compositions around $Mg_2Si_{0.4}Sn_{0.6}$ reaching $1 \leq zT_{max} \leq 1.5$ [8, 9]. However, p-type $Mg_2(Si,Sn)$ has inferior properties in comparison to n-type, partially due to a less favourable band structure, lower dominant carrier type mobility and insufficient dopant activation [10]. Recently, there has been progress on fabricating complementary p-type materials and improved $zT > 0.5$ has been observed [9, 11-13]. Zhang *et al*. reported Li doped $Mg_2Si_{0.3}Sn_{0.7}$ synthesized by solid state reaction. This composition was selected due to double valence band convergence which is good for TE properties with zT~ 0.5 [14]. Moreover, Gao *et al.*, prepared Li doped $Mg_2Si_{0.4}Sn_{0.6}$ by B_2O_3 encapsulation with zT ~ 0.7. However, the formation of MgO seems to be the cause of increasing thermal conductivity [12]. High energy ball milling has been employed to synthesize p-type $Mg_2(Si,Sn)$ reaching $zT > 0.5$ [11, 13]. This synthesis method is promising due to little or no oxidation or impurities, reduced Mg loss, and good dopant incorporation [15]. The obtained powders need to be compacted because the compaction process is important to obtain samples with good density. Its parameters such as sintering temperature and holding time affect the TE properties.

In this study, we prepared p-type Li doped $Mg_2Si_{1-x}Sn_x$ with x = 0, 0.2, 0.4, 0.6, 0.8, 1 by mechanical alloying followed by current assisted sintering. The synthesis parameters such as milling time, sintering temperature and holding time were varied to investigate the effects on TE properties. The optimal synthesis conditions were then applied to compositions with different Si:Sn ratio. Local surface mapping of the Seebeck coefficient proves that the synthesis of p-type materials for the whole compositional series is possible and furthermore allows us to correlate sample homogeneity with synthesis parameters and thermoelectric properties.

2. Materials and methods

The Li doped $Mg_2Si_{1-x}Sn_x$ with x = 0-1 solid solutions were synthesized by mechanical alloying, employing high energy ball milling (SPEX 8000D). The precursors (Mg turnings (Merck), Si (< 6mm, Chempure), Sn (< 71 μm, Merck) and Li granules with purity > 99.5%) were weighed according to nominal composition. No excess Mg was added as excess Mg can occupy the interstitial position and serve as an n-type donor [11, 16]. The desired elements were transferred into a stainless steel jar with a ball to powder ratio 1.6:1. All the procedures were conducted inside a glove box under Ar atmosphere to prevent oxidation and

contamination. The elements were milled with constant speed for 4 - 20 h until fine and homogeneous powders were obtained. The obtained fine powders were transferred to a graphite die (Ø 15 mm) and sintered at 873 - 1073 K for 600 s by utilizing DSP 510 SE from Dr. Fritsch GmbH under vacuum condition (~10^{-5} bar), under sintering pressure 66 MPa with a heating rate 1 K/ s. The density of the obtained pellets was calculated using Archimedes' method. The detailed synthesis conditions are summarized in Table 1. The obtained pellets were characterized by XRD Siemens D5000 Bragg – Brentano diffractometer with a secondary monochromator, Cu-K_α radiations (1.5406 Å) in the range (2θ: 20° - 80°) with a step size of 0.01°. The microstructure and phase purity of the samples were observed by Zeiss Ultra 55. Moreover, functional homogeneity was investigated by a spatial mapping of the Seebeck coefficient at room temperature using a PSM [17, 18].

The temperature dependent electrical conductivity and Seebeck coefficient data was obtained by a 4 probe technique [19, 20]. The thermal diffusivity (α) of the pellet was measured by using Netzsch LFA 427 apparatus. The thermal conductivity (κ) was calculated using the relation: $\kappa = \alpha \cdot \rho \cdot C_p$ where ρ and C_p are density of sample and heat capacity. The C_p value was calculated from the Dulong-Petit limit for C_v^{DP} : $C_P = C_v^{DP} + \frac{9E_t^2 T}{\beta_T \rho}$, where E_t~ 2 x 10^{-5} K^{-1} and β_T ~ 2.07 x 10^{-11} Pa^{-1} are the linear coefficient of thermal expansion and isothermal compressibility, respectively. In the relevant temperature regime C_p increases from 0.582 J/gK to 0.605 J/gK. The measurements were performed under Ar and He from 300 – 698 K. The uncertainties of measurement for S, σ, and κ are ±5%, ±5% and ±8%, respectively.

Table 1 Synthesis parameters of Li doped $Mg_2Si_{1-x}Sn_x$ with x = 0-1

Composition	Milling time (h)	T_{sinter} (K)	t_{sinter} (s)	Density (g cm^{-3})
$Mg_{1.98}Li_{0.02}Si$	6	1073	600	1.92
$Mg_{1.95}Li_{0.05}Si_{0.8}Sn_{0.2}$	20	1023	600	2.27
$Mg_{1.98}Li_{0.02}Si_{0.6}Sn_{0.4}$	20	1023	600	2.57
$Mg_{1.98}Li_{0.02}Si_{0.4}Sn_{0.6}$	20	1023	300	2.99
$Mg_{1.98}Li_{0.02}Si_{0.4}Sn_{0.6}$	20	973	300	2.95

$Mg_{1.98}Li_{0.02}Si_{0.4}S$	20	973	600	2.99
$n_{0.6}$				
$Mg_{1.98}Li_{0.02}Si_{0.4}S$	20	973	1200	2.98
$n_{0.6}$	4	923	600	3.24
$Mg_{1.98}Li_{0.02}Si_{0.2}S$	20	923	600	3.18
$n_{0.8}$				
$Mg_{1.98}Li_{0.02}Si_{0.2}S$				
$n_{0.8}$				
$Mg_{1.98}Li_{0.02}Sn$	4	873	600	3.50

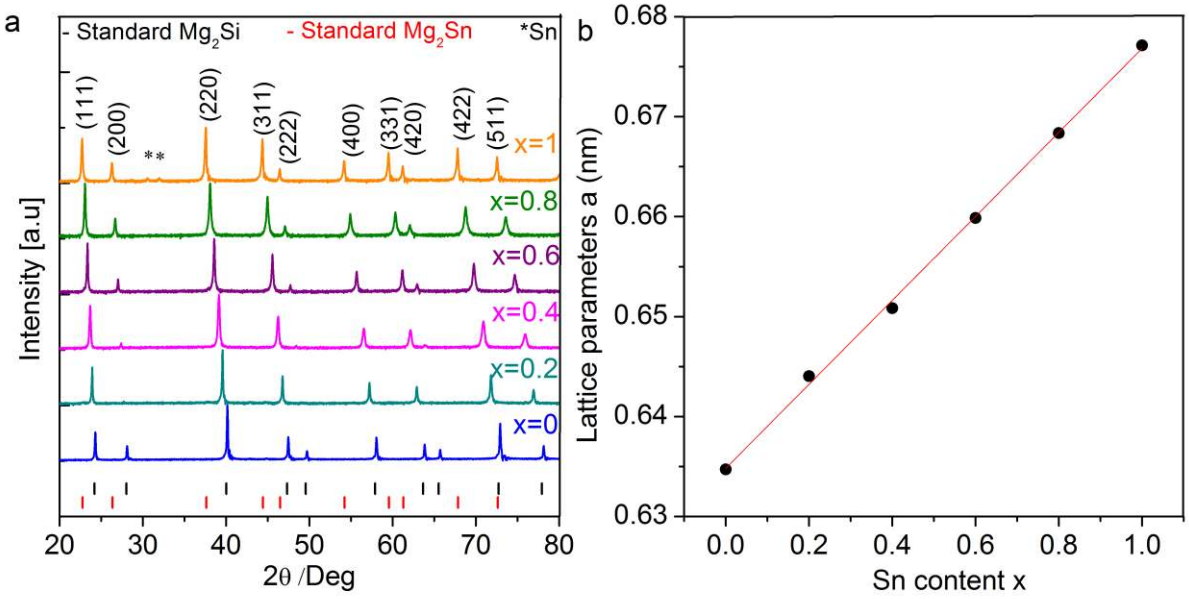

3. Results and Discussions

Fig. 1 (a) XRD pattern and (b) lattice parameters of Li doped $Mg_2Si_{1-x}Sn_x$ with x = 0-1.

The obtained pellets with relative density > 95 % except x = 0.4 (Table 1) were characterized by XRD. Fig. 1 (a) shows that all the peaks can be indexed according to the anti-fluorite structure Fm-3m space group of Mg_2Si and Mg_2Sn. The peaks gradually shift towards lower angles with increasing Sn content because Sn has larger ionic radius than Si. Within the detection limit of the XRD, all samples are single phase except Mg_2Sn, where minor peaks corresponding to elemental Sn can be found. The Sn peaks appear probably due to Mg loss. We do not observe the formation of MgO, which is often found in other synthesis routes [12,

21, 22] and detrimental for the thermoelectric properties [23]. The lattice parameter increases with increasing Sn content and rises approximately linearly, indicating that solid solutions are formed. The lattice parameter was calculated by Bragg's equation and approximately follows Vegard's rule. The results show good agreement with reference data [24].

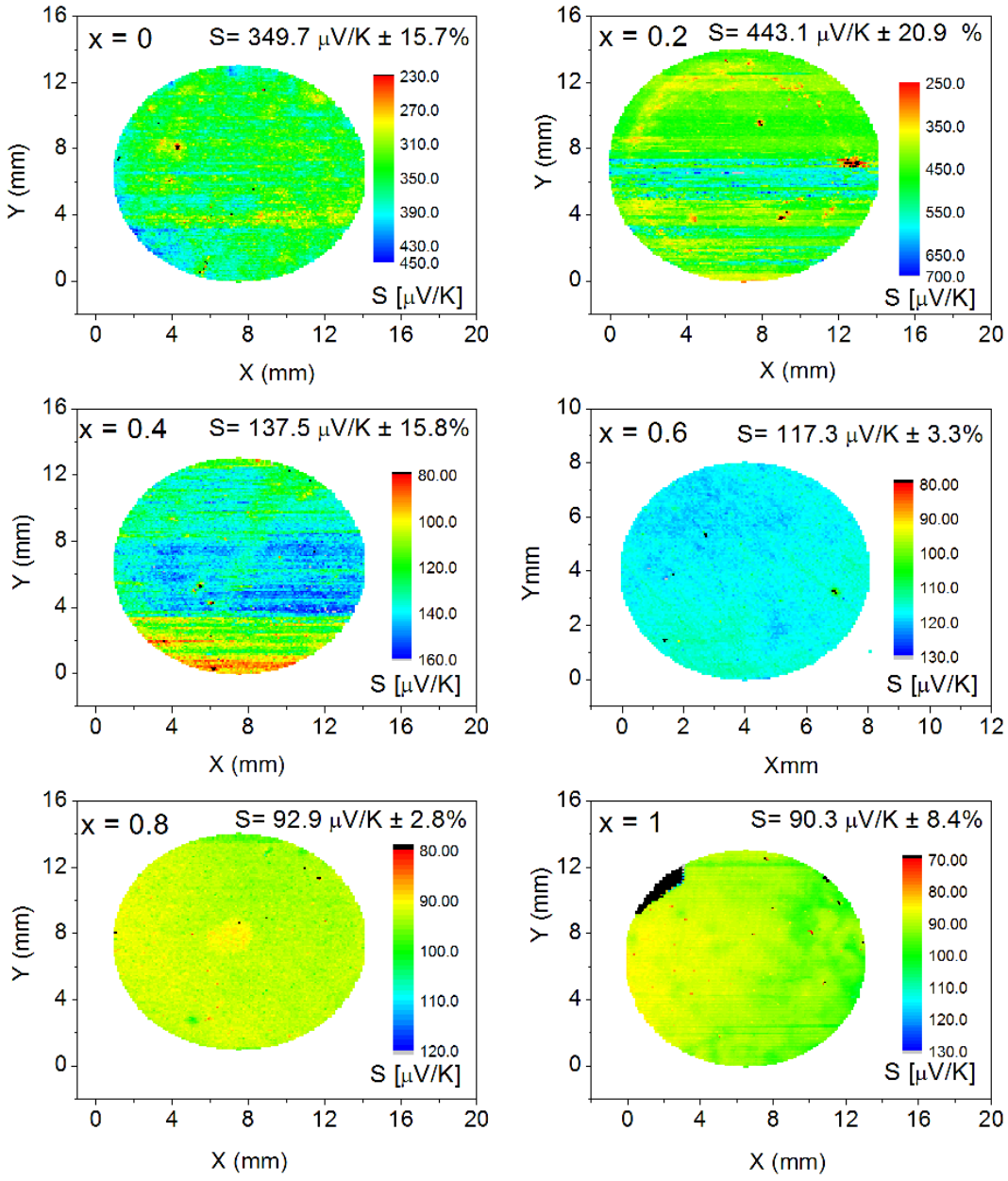

Fig. 2 Surface scan of the Seebeck coefficient of Li-doped p-type $Mg_2Si_{1-x}Sn_x$ with x = 0, 0.2, 0.4, 0.6, 0.8, and 1.

The functional homogeneity and dominant carrier type of the samples were studied by conducting surface Seebeck scans. The scanning Seebeck map shows p-type conduction for

$Mg_2Si_{1-x}Sn_x$ with x = 0, 0.2, 0.4, 0.8, and 1 (Fig. 2). For the same dopant concentration a clear decreases of S with increasing x can be observed, indicating an increasing carrier concentration (note that for the x = 0.2 has different Li concentration). This in turn points towards a dependence of dopant activation or incorporation on the Si:Sn ratio, in agreement with previous studies [25, 26] and the summarized results in a recent review [10]. The samples with low x also exhibit worse functional homogeneity, partially because local fluctuations in composition become more visible at low carrier concentration levels.

3.1 Effect of milling time on homogeneity

For the following discussion, we distinguish between the inhomogeneity in microstructure (phase purity) and inhomogeneity with respect to carrier concentration (functional). Phase purity is related to multiphase material which can be detected by SEM. The phase purity increases with increasing milling time. Based on a previous report on the same synthesis approach, the formation of compositions close to Mg_2Sn takes place within the 1 hour for n-type material [27]. Therefore, the milling time is varied between 4 and 20 hours to see the difference in microstructure. The sample with shorter milling time shows a more inhomogeneous surface (Fig. 3 (a)). Interestingly, we find that the milling time affects the

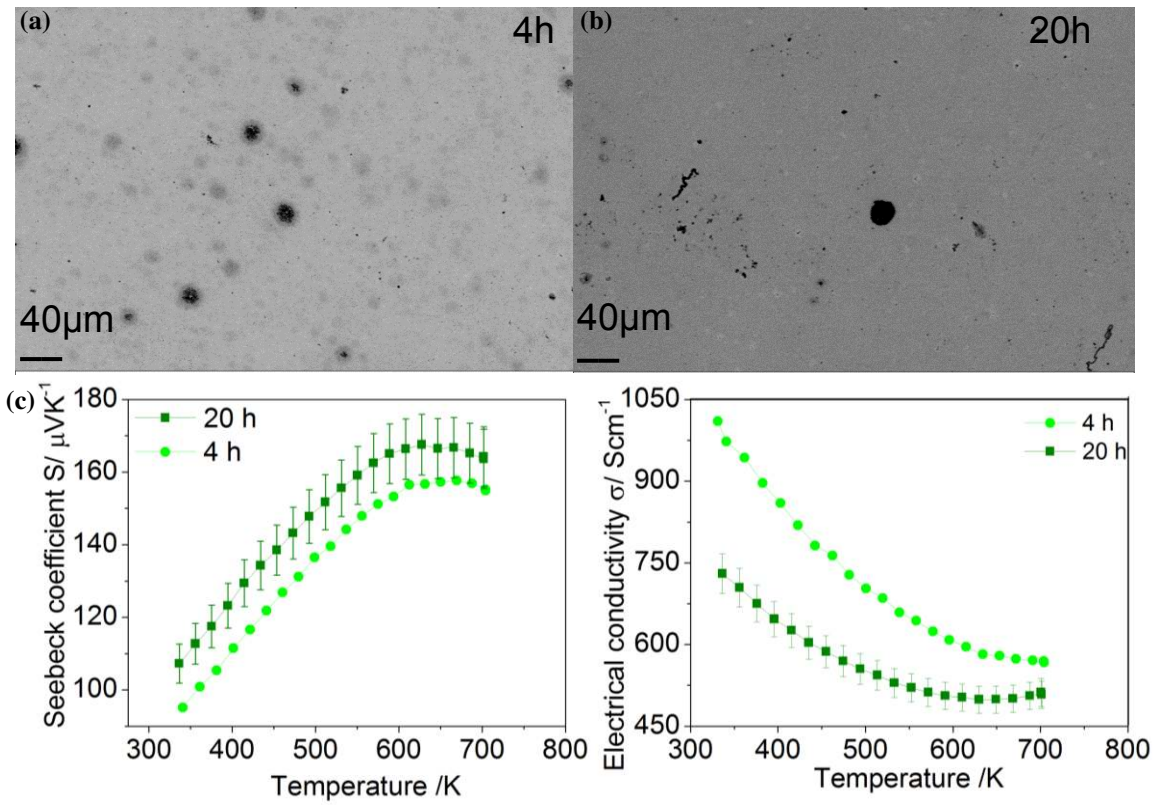

electrical conductivity of samples. The degradation of electrical conductivity with longer milling time is presumably mainly caused by carrier loss as can be deduced from the

corresponding changes in S and σ (Fig. 3 (b & c)).

The optimum milling time highly depends on Si:Sn ratio. Si rich compositions require longer milling time than Sn rich compositions because they have less ductile components [27]. On the other hand, for binary Mg_2Si, a milling duration of 6 h was found to be sufficient as also reported previously [28, 29], presumably because only one phase could be formed.

Fig. 3 SEM images of pellet $Mg_{1.98}Li_{0.02}Si_{0.2}Sn_{0.8}$ with variation of milling time (a) 4 h, (b) 20 h, and (c) TE properties.

3.2 Effects of sintering temperature and holding time on homogeneity and TE properties

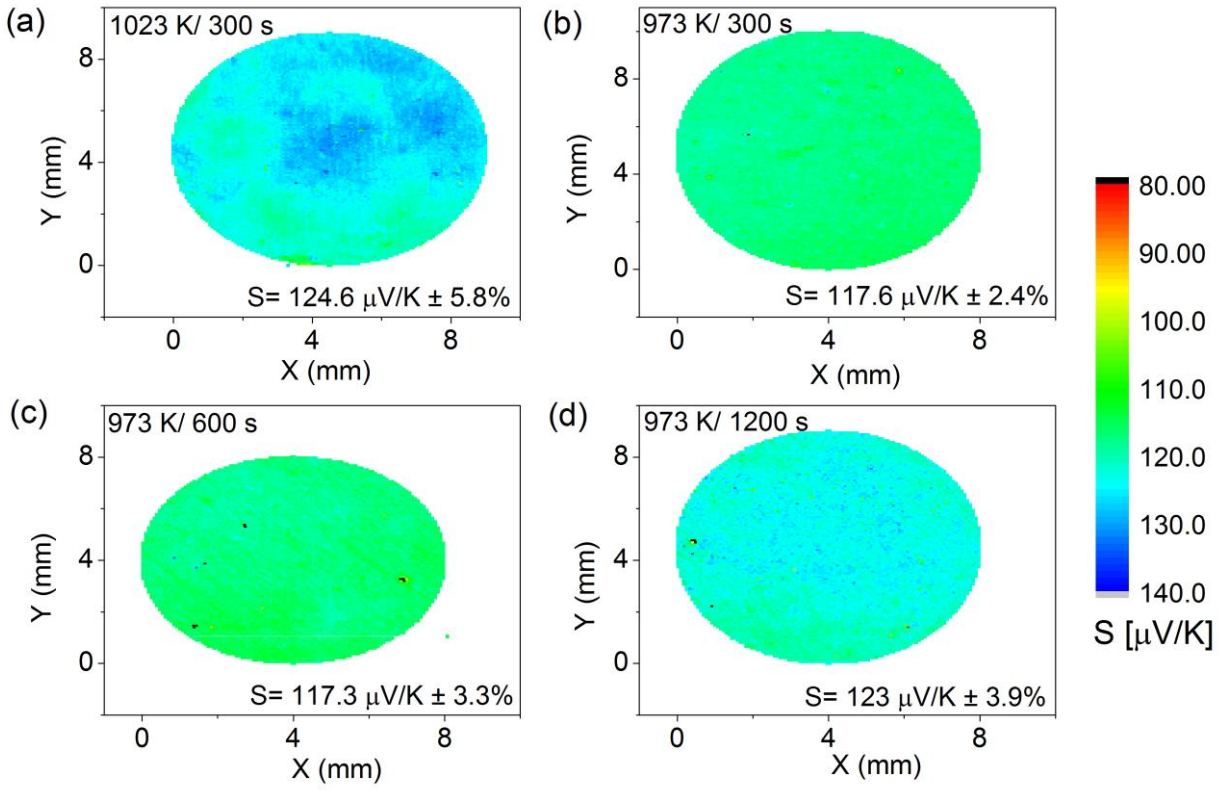

Fig. 4 Surface Seebeck scan of $Mg_{1.98}Li_{0.02}Si_{0.4}Sn_{0.6}$ at different temperature and time sintering (a) 1023 K/ 300 s, (b) 973 K/ 300 s,

(c) 973 K/ 600 s and (d) 973 K/ 1200 s.

We study the effects of sintering temperature and holding time especially in $Mg_{1.98}Li_{0.02}Si_{0.4}Sn_{0.6}$ because this composition has so far the best properties with the $zT_{max} > 0.5$ [10, 11]. Fig. 4 shows that the functional inhomogeneity in the Seebeck coefficient varies depending on sintering temperature and holding time. The functional homogeneity is quantified by the ratio of full width half maximum (FWHM) value of the Seebeck coefficient distribution and the Seebeck coefficient mean value; the lowest value corresponds to the most homogeneous one. The samples shown in Fig. 4 (b) and (c) are more homogenous than the ones shown in Fig. 4 (a) and (d). It can be deduced that longer sintering time and higher sintering temperature cause more inhomogeneous samples. The Seebeck coefficient increases slightly with increasing sintering temperature and longer holding time. However, the Seebeck coefficients of the sintered pellet at 973 K for 300 s and 600 s are the same within the measurement accuracy.

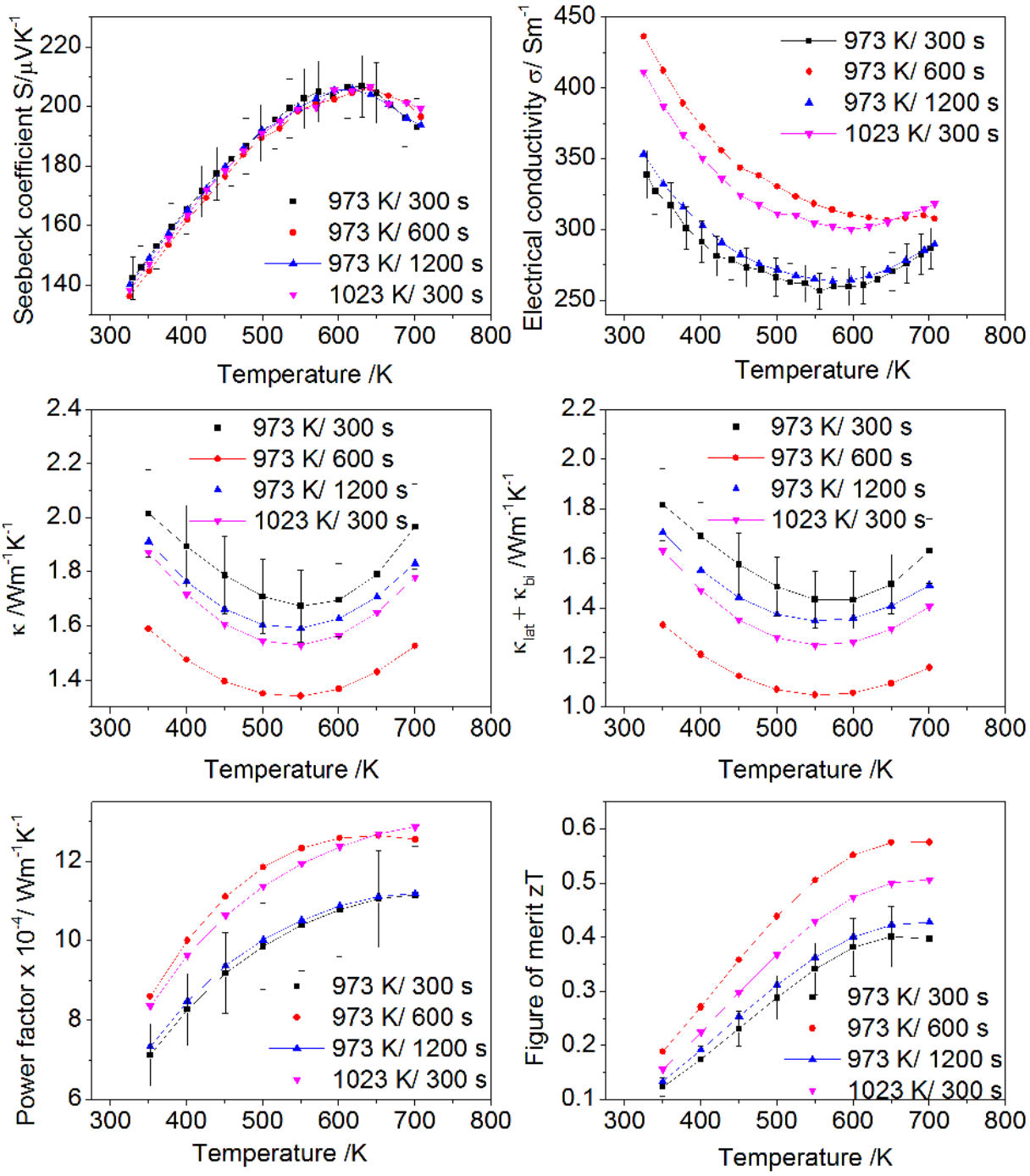

Fig. 5 Thermoelectric properties of $Mg_{1.98}Li_{0.02}Si_{0.4}Sn_{0.6}$ with different sintering temperature and time.

The integral transport properties of the $Mg_2Li_{0.02}Si_{0.4}Sn_{0.6}$ samples in the temperature range from 350 - 700 K are shown in Fig. 5. The samples exhibited colour changes on the surface after the measurement as has been mentioned previously [12]. In general, we observe a difference between the heating and the cooling data of the first measurement but good thermal stability upon further cycling. For this reason the cooling data is presented in Fig 5a) and b) and used for the calculation of power factor and *zT*. The thermoelectric figure of merit *zT* was

calculated by fitting the results for S, σ, and κ. The thermal conductivity plus bipolar contribution $(\kappa - \kappa_{el})$ was calculated from $\kappa_{lat} + \kappa_{bi} = \kappa - \kappa_{el} = \kappa - L.\sigma.T$ where κ_{el} is the electronic contribution to the thermal conductivity and the Lorenz number was calculated using the Seebeck coefficient [30]. The room temperature values corresponding to Seebeck coefficient are close to the values obtained from room temperature surface Seebeck scans. Small differences between the PSM mean value and the integral results are due to measurement principle [18]. The S is positive, indicating p-type conduction and ranges from 140 μV/K to 220 μV/K. S increases with increasing temperature as usually observed for a degenerate semiconductor and decreases at high temperature due to minority charge carriers. The observed decrease of the electrical conductivity with increasing sintering temperature and holding time is probably due to carrier loss. The electrical conductivity of the sintered pellet at 973 K/ 600 is close to 1023 K/ 300 s and the electrical conductivity of the sintered pellet at 973 K/ 300 s is close to 973 K/ 1200 s, in agreement with the trends from the Seebeck coefficients. The highest σ can be achieved for the sample sintered at 973 K /600 s which is also the most homogeneous with respect to the Seebeck scan. However, the sintered pellet at 973K /300 s has the lowest σ, although it shows a good functional homogeneity with respect to the Seebeck scan (Fig. 4). This is because the phase purity of pellet sintered at 973 K/ 300 s is lower and the sample exhibits a relatively high content of Si-rich $Mg_2(Si,Sn)$ secondary phases. These secondary phases have higher thermal conductivity [31] thus the overall lattice thermal conductivity of the sample increases. The lattice thermal conductivity shows a massive difference for 973 K/ 600s in comparison with all other samples. This sample exhibits a better phase purity possibly explaining low thermal conductivity. The power factor highly depends on electrical conductivity and decreases with longer sintering holding time at 973 K. The highest power factor of 12×10^{-4} $Wm^{-1}K^{-1}$ was obtained for sintering at 973 K/ 600 s. The figure of merit zT_{max} ~ 0.6 at 700 K is achieved. These results show that the sintering temperature and holding time play an important role in controlling the thermoelectric properties and enhancing the figure of merit zT. As discussed, we choose 973 K /600 s for an appropriate sintering temperature and holding time in $Mg_{1.98}Li_{0.02}Si_{0.4}Sn_{0.6}$.

3.3 Influence of Si:Sn ratio on sintering temperature

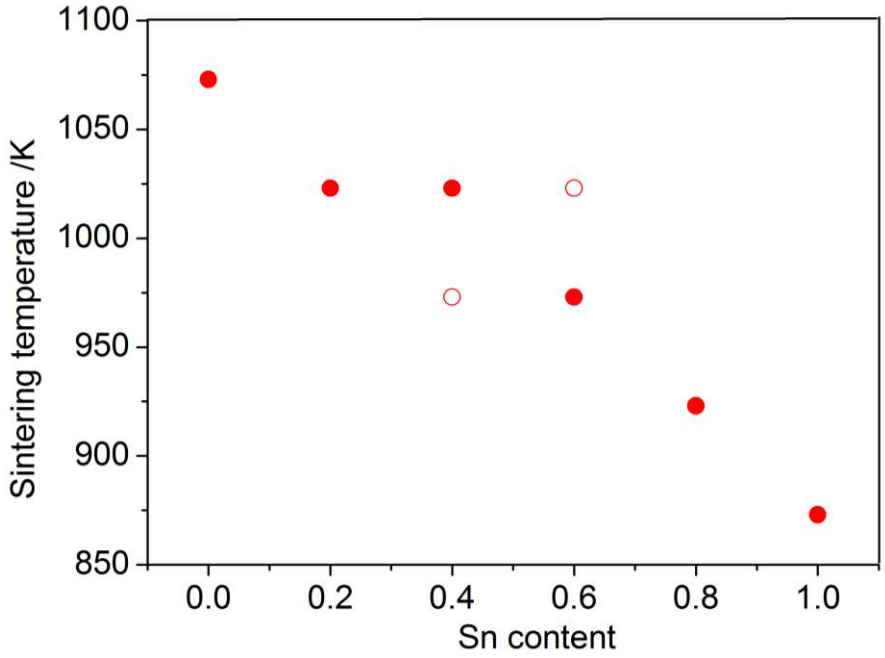

Fig. 6 Suitable sintering temperature over Sn content, the full symbol shows good properties and the empty symbol shows poor properties.

From the previous results we chose a sintering time of 600 s for all other compositions. The appropriate sintering temperature depends on the Si:Sn ratio and a suitable working window is presented in Fig. 6. As a rule of thumb a suitable sintering temperature is between 2/3 and 4/5 of the melting point of the material [32]. Determination of sintering temperature by 2/3 of melting point is a good starting point. However, others parameters should be taken such as density and starting material [32]. In our case, we find that the suitable sintering temperature is close to 4/5 of melting points of Mg_2Si (1357 K) and Mg_2Sn (1053 K) for the binary samples and the linear interpolation for the solid solutions. If sintering temperature is too high, we observed that Sn-rich material comes out of the die. On the other hand, if the sintering temperature is too low, the impurities such as Mg and Si elements can be detected with XRD and the density is lower. Moreover, it will affect TE properties, phase purity, and functional homogeneity. For example, Si rich composition with x = 0.4 at 973 K exhibits n- to p-type conduction transition corresponding to surface Seebeck scan. It shows that the sintering temperature affects the type of charge carrier. In the case of Sn rich composition with x = 0.6, a temperature difference of about 50 K leads to higher thermal conductivity and functional inhomogeneity. To sum up, an appropriate sintering temperature is crucial to optimize p-type materials.

4. Conclusion

High energy ball milling is a promising method to synthesize efficient p-type $Mg_2Si_{1-x}Sn_x$. The synthesis parameters such as milling time, sintering temperature and holding time are crucial to the optimization of the properties. They affect the phase purity, functional homogeneity and the TE properties. Local mapping of the Seebeck coefficient proves that the synthesis of p-type $Mg_2Si_{1-x}Sn_x$ with x = 0, 0.2, 0.4, 0.6, 0.8, 1 is possible for the whole compositions using Li as a dopant. The phase purity increases with longer milling time. The functional homogeneity decreases with higher sintering time and longer holding time. The optimized p-type $Mg_2Si_{0.4}Sn_{0.6}$ was achieved with zT_{max} ~ 0.6 which is comparable to the highest previously reported.

Acknowledgements

The authors would like to thank P. Blaschkewitz (DLR) for the integral thermoelectric measurements and P. Ziolkowski for support with the Seebeck scans. Also, the authors would like to gratefully acknowledge the endorsement from the DLR Executive Board Member for Space Research and Technology and the financial support from the Young Research Group Leader Program. Furthermore, financial support of one of the authors (M. Yasseri) is provided by the DFG via GRK 2204.

References

[1] R.C. O'Brien, R.M. Ambrosi, N.P. Bannister, S.D. Howe, H.V. Atkinson, Journal of Nuclear Materials 377 (2008) 506-521.

[2] B. Orr, A. Akbarzadeh, M. Mochizuki, R. Singh, Applied Thermal Engineering 101 (2016) 490-495.

[3] S. LeBlanc, S.K. Yee, M.L. Scullin, C. Dames, K.E. Goodson, Renewable & Sustainable Energy Reviews 32 (2014) 313-327.

[4] M.W. Gaultois, T.D. Sparks, C.K.H. Borg, R. Seshadri, W.D. Bonificio, D.R. Clarke, Chemistry of Materials 25 (2013) 2911-2920.

[5] J. de Boor, T. Dasgupta, E. Mueller, Thermoelectric Properties of Magnesium Silicide Based Solid Solutions and Higher Manganese Silicides, in: C. Uher (Ed.) Materials Aspect of Thermoelectricty, Taylor & Francis, 2016.

[6] J. Zhao, Z. Liu, J. Reid, K. Takarabe, T. Iida, B. Wang, U. Yoshiya, J.S. Tse, Journal of Materials Chemistry A 3 (2015) 19774-19782.

[7] G. Kim, H. Lee, J. Kim, J.W. Roh, I. Lyo, B.-W. Kim, K.H. Lee, W. Lee, Scripta Materialia 128 (2017) 53-56.
[8] V.K. Zaitsev, Thermoelectrics on the Base of Solid Solutions of Mg2BIV Compounds (BIV = Si, Ge, Sn), Thermoelectrics Handbook, CRC Press, 2005, pp. 29-21-29-12.
[9] P. Gao, I. Berkun, R.D. Schmidt, M.F. Luzenski, X. Lu, P. Bordon Sarac, E.D. Case, T.P. Hogan, Journal of Electronic Materials 43 (2014) 1790-1803.
[10] J. de Boor, T. Dasgupta, U. Saparamadu, E. Mueller, Z.F. Ren, Materials Today Energy 4 (2017) 105-121.
[11] J. de Boor, U. Saparamadu, J. Mao, K. Dahal, E. Mueller, Z. Ren, Acta Materialia 120 (2016) 273-280.
[12] P. Gao, J.D. Davis, V.V. Poltavets, T.P. Hogan, Journal of Materials Chemistry C 4 (2016) 929-934.
[13] U. Saparamadu, J. de Boor, J. Mao, S. Song, F. Tian, W. Liu, Q. Zhang, Z. Ren, Acta Materialia 141 (2017) 154-162.
[14] Q. Zhang, L. Cheng, W. Liu, Y. Zheng, X. Su, H. Chi, H. Liu, Y. Yan, X. Tang, C. Uher, Physical Chemistry Chemical Physics 16 (2014) 23576-23583.
[15] C. Suryanarayana, Progress in Materials Science 46 (2001) 1-184.
[16] X. Liu, L. Xi, W. Qiu, J. Yang, T. Zhu, X. Zhao, W. Zhang, Advanced Electronic Materials 2 (2016) 1500284-n/a.
[17] D. Platzek, G. Karpinski, C. Stiewe, P. Ziolkowski, C. Drasar, E. Mueller, Potential-Seebeck-Microprobe (PSM): Measuring the spatial resolution of the Seebeck coefficient and the electric potential, ICT: 2005 24th International Conference on Thermoelectrics, Ieee, New York, 2005, pp. 13-16.
[18] P. Ziolkowski, G. Karpinski, T. Dasgupta, E. Mueller, Physica Status Solidi a-Applications and Materials Science 210 (2013) 89-105.
[19] J. de Boor, C. Stiewe, P. Ziolkowski, T. Dasgupta, G. Karpinski, E. Lenz, F. Edler, E. Mueller, Journal of Electronic Materials 42 (2013) 1711-1718.
[20] J. de Boor, E. Mueller, Review of Scientific Instruments 84 (2013) 065102.
[21] J. de Boor, C. Compere, T. Dasgupta, C. Stiewe, H. Kolb, A. Schmitz, E. Mueller, Journal of Materials Science 49 (2014) 3196-3204.
[22] T. Dasgupta, C. Stiewe, R. Hassdorf, A.J. Zhou, L. Boettcher, E. Mueller, Physical Review B 83 (2011) 235207.
[23] J. de Boor, T. Dasgupta, H. Kolb, C. Compere, K. Kelm, E. Mueller, Acta Materialia 77 (2014) 68-75.

[24] R.B. Song, T. Aizawa, J.Q. Sun, Materials Science and Engineering: B 136 (2007) 111-117.

[25] S. Kim, B. Wiendlocha, H. Jin, J. Tobola, J.P. Heremans, Journal of Applied Physics 116 (2014) 153706.

[26] G.N. Isachenko, A.Y. Samunin, E.A. Gurieva, M.I. Fedorov, D.A. Pshenay-Severin, P.P. Konstantinov, M.D. Kamolova, Journal of Electronic Materials 45 (2016) 1982-1986.

[27] A. Sankhla, A. Patil, H. Kamila, M. Yasseri, N. Farahi, E. Mueller, J. de Boor, ACS Applied energy Materials (2018) DOI: 10.1021/acsaem.7b00128.

[28] S.K. Bux, M.T. Yeung, E.S. Toberer, G.J. Snyder, R.B. Kaner, J.-P. Fleurial, Journal of Materials Chemistry 21 (2011) 12259-12266.

[29] T. Ikeda, L. Haviez, Y. Li, G.J. Snyder, Small 8 (2012) 2350-2355.

[30] H.-S. Kim, Z.M. Gibbs, Y. Tang, H. Wang, G.J. Snyder, APL Materials 3 (2015) 041506.

[31] P. Bellanger, S. Gorsse, G. Bernard-Granger, C. Navone, A. Redjaimia, S. Vivès, Acta Materialia 95 (2015) 102-110.

[32] A.A. Bondi, (1968).